International Journal of Optomechatronics
Publication details, including instructions for authors and subscription information:
http://www.informaworld.com/smpp/title~content=t741771165

Photothermal Tuning and Size Locking of Salt-Water Microdroplets on a Superhydrophobic Surface

Michael Mestre [a]; Yasin Karadag [a]; S. Cigdem Yorulmaz [a]; Mustafa Gündoğan [a]; Alper Kiraz [a]
[a] Department of Physics, Koç University, Istanbul, Turkey

Online publication date: 20 November 2009

To cite this Article Mestre, Michael, Karadag, Yasin, Yorulmaz, S. Cigdem, Gündoğan, Mustafa and Kiraz, Alper(2009) 'Photothermal Tuning and Size Locking of Salt-Water Microdroplets on a Superhydrophobic Surface', International Journal of Optomechatronics, 3: 4, 303 — 318
To link to this Article: DOI: 10.1080/15599610903391176
URL: http://dx.doi.org/10.1080/15599610903391176

International Journal of Optomechatronics, 3: 303–318, 2009

ISSN: 1559-9612 print/1559-9620 online
DOI: 10.1080/15599610903391176

PHOTOTHERMAL TUNING AND SIZE LOCKING OF SALT-WATER MICRODROPLETS ON A SUPERHYDROPHOBIC SURFACE

Michael Mestre, Yasin Karadag, S. Cigdem Yorulmaz, Mustafa Gündoğan, and Alper Kiraz
Department of Physics, Koç University, Istanbul, Turkey

Liquid microdroplets are attractive as optical microcavities with tunable resonances for applications in quantum optics and biological sensing, owing to their flexible nature and spherical shape. Salt-water microdroplets can be used in such experiments while standing on a superhydrophobic surface that preserves their spherical geometry. Here, we report how the photothermal effect enables continuous tuning or locking of the whispering gallery mode (WGM) spectrum and size of salt-water microdroplets on a superhydrophobic surface. Local heating by an infrared laser focused at the center of a microdroplet causes it to depart from its equilibrium size, shifting the WGM spectrum. This photothermal tuning effect is fully reversible and can be used to tune the microdroplet radius with a precision reaching 1Å. We combine this effect with fluorescence excitation spectroscopy using a fixed wavelength laser to measure Q-factors of up to $\sim 10^5$. Conversely, focusing the heating laser to the microdroplet rim reveals absorption resonances, leading to a hysteretic behavior when cycling the laser power. We show that this behavior can be used to lock the size of a microdroplet and make it exhibit optical bistability. WGM resonances of locked microdroplets are probed using a tunable laser, showing a spectral locking precision reaching <0.01 nm over tens of minutes. These results indicate that the wavelength stability and positioning challenges inherent to liquid microdroplets in air can be overcome, providing an easily tunable and lockable alternative to solid optical microcavities and making them potential candidates for studies in cavity optomechanics.

Keywords: absorption resonance, fluorescence excitation spectroscopy, microdroplet, optical bistability, Q-factor, self-stability, superhydrophobic surface, whispering gallery mode

1. INTRODUCTION

Liquid microdroplets have a spherical shape, smooth surface, and flexible nature. These unique properties make them attractive for various applications in quantum optics and biological sensing that especially require a high quality optical microcavity with tunable resonances (Vahala 2003; Fields et al. 2000; Reid et al. 2007). They host high quality optical resonances named whispering gallery modes (WGMs). In addition to enabling enhanced optical interactions, WGMs serve as exquisitely sensitive probes of the size and refractive index of the microdroplet. The

Address correspondence to Alper Kiraz, Department of Physics, Koç University, Rumelifeneri Yolu, 34450 Sariyer, Istanbul, Turkey. E-mail: akiraz@ku.edu.tr

NOMENCLATURE

a	microdroplet radius	$P_A^0(T)$	vapor pressure of water at temperature T
$c_{A,s}$	molar concentration of water at the surface of the microdroplet	Q	WGM resonance quality factor
$c_{A,\infty}$	molar concentration of water in the bulk gas	$\widetilde{Q}_{\text{abs}}$	ratio of total power absorbed by the droplet to total power of incident beam
C_{PL}	molar heat capacity of the microdroplet	R	universal gas constant
D_A	gas phase diffusion coefficient of water in air	S_A	relative water humidity in the chamber
f_{PB}	correction factor from the Picknett and Bexon equation	Sh_A	Sherwood number for the microdroplet
k_{eff}	area average of the heat conductivities of air and substrate	t	time
n	water refractive index at 1064 nm	T_∞	chamber temperature far from the microdroplet
N	total number of moles in the microdroplet (salt + water)	T_d	air-microdroplet interface temperature
N_A	number of moles of water in the microdroplet	w_0	Gaussian beam focal waist
NA	microscope numerical aperture	x_A	mole fraction of water
P_{inc}	total power of incident beam	$\alpha = 2\pi a/\lambda$	microdroplet size parameter
		γ_A	activity coefficient of water
		Δx	infinitesimal variation of x
		$\Delta H_{\text{vap},A}$	latent heat of vaporization of water
		λ	wavelength of incident light
		ρ	solution density

asymptotically linear relationship between the spectral positions of the WGMs and the spherical radius ($\Delta\lambda/\lambda = \Delta r/r$) dictates the high sensitivity in determining the size change of a microdroplet by spectral tracing of the WGMs (Qian et al. 1986).

The results presented here demonstrate the precise control and stabilization of the size of salt-water microdroplets using the photothermal effect. In both cases, spectral positions of the WGMs are employed in determining the size of the microdroplets with a precision reaching 1 Å. The experiments are performed on salt-water microdroplets that are standing on a superhydrophobic surface in the controlled atmosphere of a constant-humidity chamber. This experimental configuration preserves the sphericity of the microdroplets while enabling their complete position stabilization (Kiraz et al. 2006).

Photothermal tuning relies on local heating of a water microdroplet that contains a nonvolatile component, such as glycerol or salt, with a focused infrared laser. We have recently demonstrated that photothermal tuning can be used in large, almost reversible spectral tuning of the whispering gallery modes (WGMs) of liquid microdroplets (Kiraz et al. 2008, 2009). We have also demonstrated that a hysteretic behavior can be observed in a photothermal tuning cycle when the infrared laser is focused near the rim of the microdroplet, enabling bistable operation (Karadag et al. 2009). The observed hysteresis loops also reveal operation points where the volume of the liquid microdroplet can be self-stabilized. Here, we present the results of two recent fluorescence excitation experiments performed in our laboratory. In the first case, fluorescence from a microdroplet is recorded as its size is precisely tuned using photothermal tuning. This technique described in Section 4, enables the observation of WGMs with a spectral resolution of <0.01 nm. The second fluorescence excitation experiment that we present relies on measuring

the WGMs of size-locked microdroplets using a tunable laser. Our results showing size stabilization better than 1 Å are summarized in Section 5.

2. MODELIZATION AND SIMULATION

A lumped system model which assumes that all of the variables of the salt-water microdroplet and the chamber are uniform throughout their whole respective volumes is used for photothermal tuning (Kiraz et al. 2008, 2009). The rate of change of the number of moles of water (N_A) in the microdroplet is given as (Ray et al. 1989),

$$\frac{dN_A}{dt} = -2\pi a \,\mathrm{Sh}_A D_A \left(c_{A,s} - c_{A,\infty}\right) \tag{1}$$

The Sherwood number Sh_A reduces to 2 in our case due to the absence of flow. After taking into account the influence of the surface on the diffusion rate with the corrective term f_{pb} (Picknett and Bexon 1977) and substituting the terms, an expression is obtained where the relative water humidity in the chamber (S_A) and the water vapor pressure at the surface of the droplet (governed by the activity coefficient γ_A) determine the rate of change of N_A via

$$\frac{dN_A}{dt} = -4\pi a f_{PB} D_A \frac{P_A^0(T_\infty)}{RT_\infty} \left(\gamma_A x_A \phi_A - S_A\right) \tag{2}$$

where

$$\phi_A = \frac{P_A^0(T_d)}{P_A^0(T_\infty)} \left(\frac{T_\infty}{T_d}\right) \tag{3}$$

The temperature change in the microdroplet due to the evaporation of water, conductive heat loss, and photothermal heating is given as

$$\frac{dT_d}{dt} = \frac{dN_A}{dt} \frac{\Delta H_{\mathrm{vap},A}}{NC_{PL}} - \frac{3k_{\mathrm{eff}} V_m}{a^2 C_{PL}} (T_d - T_\infty) + \frac{\widetilde{Q}_{\mathrm{abs}} P_{\mathrm{inc}}}{NC_{PL}} \tag{4}$$

In Eqs. (1)–(4), Sh_A is the Sherwood number for the microdroplet; D_A is the molecular diffusivity in the gas mixture; $c_{A,s}$ and $c_{A,\infty}$ are the molar concentrations of water at the surface of the droplet and far from it, respectively; x_A is the mole fraction of water; R is the universal gas constant; $P_A^0(T)$ is the vapor pressure at temperature T; T_d and T_∞ are the temperatures at the air-microdroplet interface and in the chamber far from the microdroplet; $\Delta H_{\mathrm{vap},A}$ is the latent heat of vaporization of water; N is the total number of moles in the microdroplet; V_m is the molar specific volume; C_{PL} is the molar heat capacity of the microdroplet mixture; k_{eff} is the area average of the heat conductivities of the air and the substrate (Kiraz et al. 2009); and $\widetilde{Q}_{\mathrm{abs}}$ is the ratio of the total power absorbed by the droplet to the total power of the incident beam (P_{inc}), respectively. The correction factor f_{PB} is calculated by using the Picknett and Bexon (Picknett and Bexon 1977; McHale et al. 2005) equation assuming a typical contact angle of $\theta = 160°$. The water activity coefficient (γ_A) and solution density (ρ) in g/cm^3 of NaCl-water microdroplets are computed using the

polynomial best fit coefficients given in Tang et al. (1997). In the simulations, C_{PL} is also dynamically calculated as a function of the salt concentration (The Engineering Toolbox 2009).

The localized approximation to the generalized Lorenz–Mie theory is applied for the calculations of the modified absorption ($\widetilde{Q}_{\mathrm{abs}}$) of a Gaussian beam focused at the center or near the rim of the microdroplet (Lock and Gouesbet 1994; Gouesbet and Lock 1994). $\widetilde{Q}_{\mathrm{abs}}$ is the ratio of the total power absorbed by the microdroplet to the total power of the incident beam. Figure 1 shows the results of the $\widetilde{Q}_{\mathrm{abs}}$ calculations as a function of the size parameter $\alpha = 2\pi a/\lambda$, where a and λ are the radius of the microdroplet and wavelength, respectively. The refractive index of the microdroplet is assumed to be $n = 1.3544 + 1112.15 \cdot 10^{-9} i$ in these calculations, considering the equilibrium NaCl concentration of 3.83 M in the microdroplet

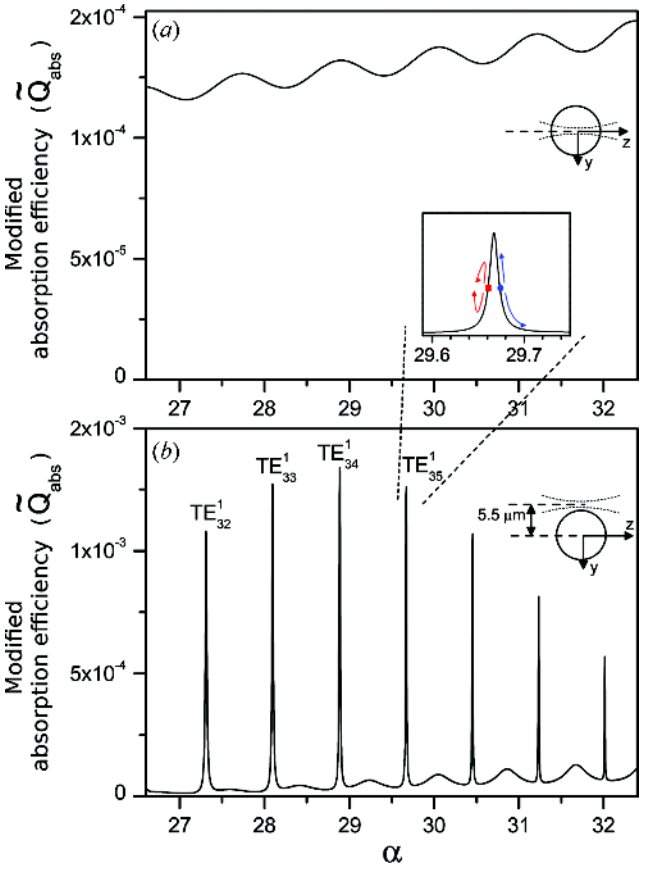

Figure 1. Modified absorption efficiency ($\widetilde{Q}_{\mathrm{abs}}$) as a function of the size parameter (α) assuming a spherical particle suspended in air. (*a*) On-axis illumination—the infrared laser is focused to the center of the particle. Low quality oscillations correspond to Fabry–Perot resonances; and (*b*) Off-axis illumination—the infrared laser is focused near the rim of the spherical particle at $y = 5.5\,\mu\mathrm{m}$. Inset shows the absorption resonance around $\alpha = 29.66$. The red square and blue disk indicate the stable and unstable operation points, respectively. (Figure is provided in color online.)

(Karadag et al. 2009). A Gaussian beam with a focal waist of $w_0 = 1000\,\text{nm}$ that is propagating along z and linearly polarized along x directions is considered. Figure 1(a) considers on-axis illumination, i.e., the beam is focused at the center of the microdroplet. WGMs are therefore not excited in this configuration; only low quality oscillations corresponding to Fabry–Perot resonance modes are observed (Kiraz et al. 2008). This experimental configuration allows for almost linear and reversible size tuning of the microdroplets and is used for the photothermal tuning spectroscopy experiments described in Section 4. In contrast, WGMs are clearly visible in Figure 1(b), where the beam is assumed to be focused near the rim, 5.5 μm away from the microdroplet's center along the y direction. Polarization, angular momentum number, and radial mode order of the WGMs are also shown in the figure. Due to the selected focal point and Gaussian beam polarization only TE WGMs are excited (Fields et al. 2000). The resonances lead to a hysteretic behavior for the microdroplet size and WGM spectrum when the heating laser power is increased and decreased in a cycle (Karadag et al. 2009), enabling bistable switching of the WGM spectral shift. Furthermore, this experimental configuration is used for the size locking experiments described in Section 5. The essence of the self-stabilization effect is shown in the inset in Figure 1. During a photothermal

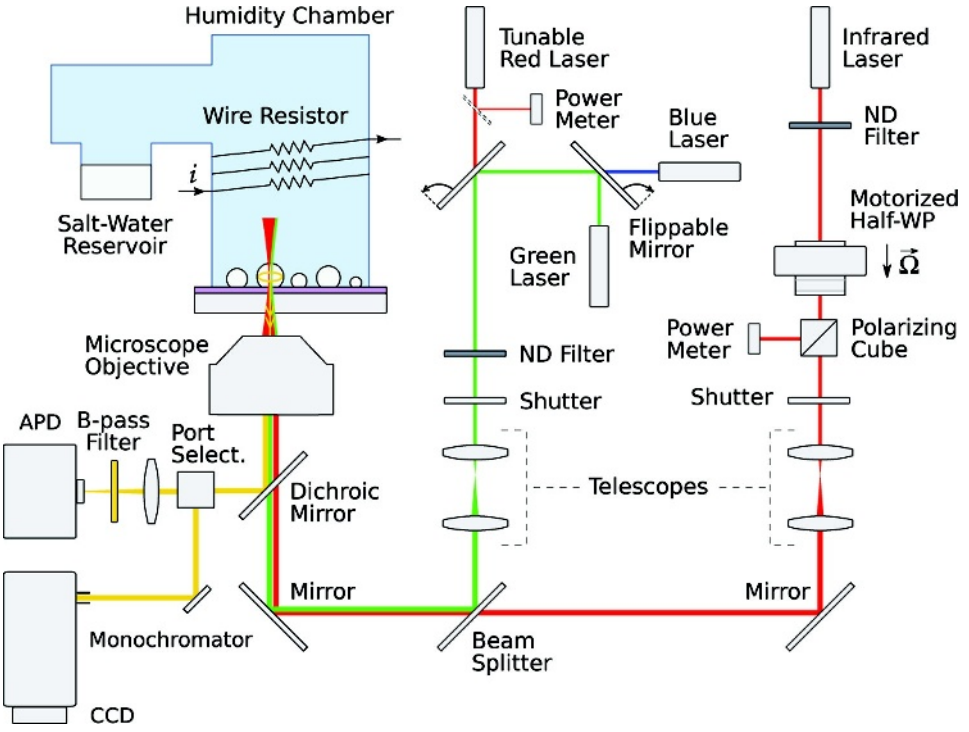

Figure 2. Optical setup and the humidity chamber. The microdroplets rest on the superhydrophobic surface at the bottom of the humidity chamber; the salt-water reservoir ensures a stable humidity level. The flippable mirrors enable to select the probe laser (tunable red external cavity, green or blue). The fluorescence light is directed either to the Avalanche Photodiode (APD) or to the monochromator, depending on the port selector position at the microscope output. (Figure is provided in color online.)

tuning cycle where the heating laser power is first increased and then decreased, self-stable operation points can be found if the cycle contains a WGM absorption resonance. Around a self-stable operation point (shown as the red square in the inset in Figure 1), the decrease (increase) in the heating laser power is compensated by the increase (decrease) in $\widetilde{Q}_{\mathrm{abs}}$.

3. SAMPLE PREPARATION AND EXPERIMENTAL SETUP

The experimental setup is illustrated in Figure 2. Experiments are performed on NaCl-water microdroplets (diameters 5–15 μm) doped with 1–50 μM rhodamine B or rhodamine 700 that are standing on a superhydrophobic surface and kept in a chamber with stable relative humidity. Superhydrophobic surfaces are prepared by spin coating silica nanoparticles on a cover glass (Kiraz et al. 2008). Microdroplets are sprayed on the superhydrophobic surface with an ultrasonic nebulizer. A solid state infrared laser ($\lambda = 1064$ nm) is used for photothermal tuning. The infrared laser power (P_{inc}) is adjusted by rotating a $\lambda/2$ waveplate placed before a polarizing beam splitter using a stepper motor with 3,300 steps per half revolution. P_{inc}, therefore, changes following a sinusoidal curve going from maximum to minimum in 1,650 steps. A green solid state laser ($\lambda = 532$ nm), a blue Argon-ion laser ($\lambda = 488$ nm), or a tunable red external cavity diode laser ($\lambda = 632$–637 nm, New Focus TLB-6304) is used for exciting the dye molecules in the microdroplets. Excitation lasers are focused at an individual microdroplet in the inverted geometry using a high NA microscope objective (NA = 1.4, 60×) which is also used to collect the fluorescence. A 50 cm monochromator and a CCD camera are used to record the conventional fluorescence spectra of the microdroplets (spectral resolution ~0.15 nm). Band-pass filters and an avalanche photodiode (APD) are used to detect the fluorescence intensity for photothermal tuning spectroscopy experiments, and those using the tunable laser.

4. SPECTROSCOPY USING PHOTOTHERMAL TUNING

Scanning Fabry–Perot interferometers are equipped with a piezoelectric actuator onto which one of the two mirrors is mounted. When the voltage applied to the actuator is ramped, the cavity length is finely tuned. By measuring the transmission of a fixed frequency incident laser beam through the Fabry–Perot cavity, the cavity resonances are observed. Here, we measure the WGMs of microdroplets in a similar way. Our measurements rely on the ability to control finely and reversibly the evaporation/condensation of salt-water microdroplets in the sealed humidity chamber. By focusing the infrared laser beam onto the center of an individual microdroplet (on-axis illumination), its size is photothermally tuned in a reversible way. The amount of photothermal tuning is determined by the specific salt in the microdroplet and the relative water humidity of the chamber (Kiraz et al. 2008, 2009). Just like in the case of a Fabry–Perot cavity, this size change leads to a shift in the resonance frequencies. A photothermal tuning spectrum is then obtained by integrating photon counts from the APD that records the fluorescence emitted by the dye-doped microdroplet as the intensity of the infrared laser is changed step by step using the stepper motor described in Figure 2. While the APD monitors the light intensity at around the fluorescence wavelength ($\lambda_f \simeq 590$ nm in this case for

rhodamine B), the recorded signal is in fact proportional to the absorption of the probe laser ($\lambda_p = 488\,\text{nm}$) by the microdroplet. Hence, our measurements are similar to the well-known fluorescence (or photoluminescence) excitation spectroscopy (Orrit and Bernard 1990).

A calibration of the relative wavelength shift versus the heating laser power is performed for each microdroplet using our conventional spectrometer (Figure 2). In these measurements, the spectral position of a WGM peak, hence the relative wavelength shift, is recorded at different P_{inc} values. Figure 3 shows the calibration curves obtained on the same day from four different microdroplets with diameters ranging from 9–15 μm. As expected from the previous results (Kiraz et al. 2008, 2009), almost linear relationships are observed between P_{inc} and the relative wavelength shift, and microdroplets with different diameters located in the same environment exhibit little difference in their calibration curves shown in Figure 3. Calibration slopes between $-4.61\,\text{nm/mW}$ and $-4.27\,\text{nm/mW}$ are observed for these microdroplets for the fluorescence wavelength $\lambda_f \simeq 590\,\text{nm}$. The slope at the probe laser wavelength $\lambda_p = 488\,\text{nm}$ is obtained by multiplying the values with the ratio λ_p/λ_f, taking into account the asymptotically linear relationship between the normalized drifts in the spectral position of a WGM and the microdroplet radius $\Delta\lambda/\lambda = \Delta a/a$ (Tzeng et al. 1984).

The linear relationship between the spectral drift of the WGMs and the infrared laser power is verified with calculations performed using the thermodynamic model described in Section 2. In these calculations, the infrared laser power is ramped in discrete steps in a way similar to what the stepper motor performs in our setup. The calculated spectral drifts observed in the WGMs at around 488 nm are plotted in Figure 4 as a function of time and infrared laser

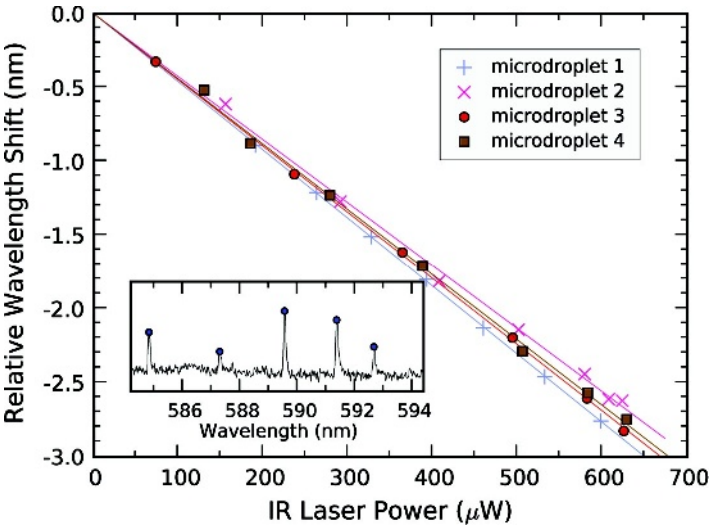

Figure 3. Relative WGM wavelength shift with respect to the infrared laser power for different microdroplets (diameters between 9–15 μm) at the fluorescence wavelength $\lambda_f \simeq 590\,\text{nm}$. Inset shows a sample spectrum from the monochromator for microdroplet 1 used to plot one data point. (Figure is provided in color online.)

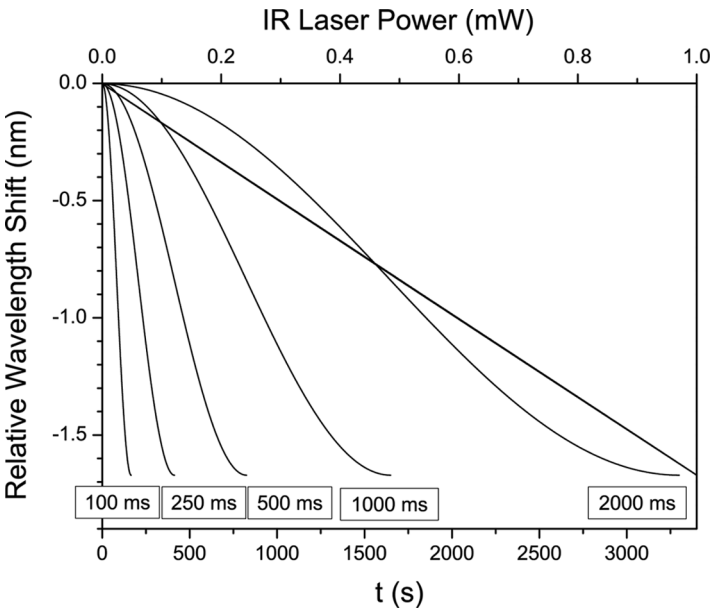

Figure 4. Calculated relative WGM wavelength shift from a 12 μm diameter microdroplet as a function of time and infrared laser power, considering different integration times of 100, 250, 500, 1000, and 2000 ms. The sinusoidal curves show the relative wavelength shifts calculated as a function of time as the infrared laser power is increased as in the experiment. The linear curves show the calculated relative wavelength shifts as a function of the infrared laser power using different integration times. The linear curves almost fully overlap for the selected integration times.

power for different integration times. Calculations are time-resolved between the steps, meaning that it is not assumed that an asymptotic equilibrium is reached between each step. Despite this, the tuning curves obtained in this fashion are highly linear; furthermore, the tuning range is almost constant when the step interval is $\geq$100 ms. Lower values of the step interval lead to a decreased tuning range as well as a degradation of the linearity between the relative wavelength shift and the infrared laser power. This result leads us to conclude that microdroplet tunability is continuous and linear to a very good approximation, provided that a sufficiently long integration time ($\geq$100 ms) elapses between consecutive stepper motor positions. We note that a deviation is observed between the relative wavelength shifts calculated in Figure 4 and experimentally observed in Figure 3 at a given infrared laser power. This deviation, which is due to the inaccuracies of the parameters assumed in the thermodynamical model, does not have an impact on the expected time scales. Furthermore, it can be noted that according to previous calculations, the temperature change induced by such a tuning inside microdroplets should not exceed 1 K (Kiraz et al. 2008).

The resolution of our measurements is imposed by the precision to which we can adjust the infrared laser power. Due to the sinusoidal shape of the power tuning curve, this resolution is not constant across the tuning range. For the stepper motor used in our setup (3,300 steps per half-turn), at the position where the rate of change of the infrared laser power is maximum (and, therefore, where the

resolution is the lowest), the power tuning precision is 9.5×10^{-4} $\Delta\lambda_{max}$, where $\Delta\lambda_{max}$ denotes the magnitude of the maximum spectral drift observed for the maximum available infrared laser power. For typical values of the wavelength shift calibration measurements in our microdroplets (as in Figure 3), this leads to a wavelength tuning precision of $\sim$0.002 nm, taking into account the maximum infrared laser power of 625 μW used in our experiments. This corresponds to a spectral resolution of $\sim$0.004 nm, considering that three data points should be recorded to resolve a peak. Similarly, a measurement near the edge of the power tuning curve where the rate of change of the infrared laser power is smaller leads to a higher photothermal tuning resolution. For instance, at a phase angle of $\pi/6$ on the cosine, the power tuning precision is 4.75×10^{-4} $\Delta\lambda_{max}$ corresponding to a spectral resolution of $\sim$0.002 nm in our experimental conditions.

Microdroplets with a larger contact angle were selected by visual inspection of the microscope images, especially when aiming to measure high Q-factors. Photothermal tuning spectroscopy experiments performed on such microdroplets commonly revealed peaks with Q-factors within the range of 40,000–100,000. Furthermore, most of the times, these peaks did not exhibit the lifting of the azimuthal degeneracy which is a characteristic of spheroidal deformations of microdroplets (Yorulmaz et al. 2009). This indicates that the associated microdroplets had good sphericity.

Figure 5 shows the photothermal spectra recorded from a 12 μm diameter microdroplet giving one of the highest Q-factors that we have measured ($Q \simeq$ 95,000), together with the associated wavelength calibration curve (Figure 5*a*). The photothermal spectrum shown in Figure 5(*b*) is recorded using an integration time of 250 ms. The Lorentzian fit made to the WGM peak observed at around -0.5 nm relative wavelength shift in this spectrum reveals a FWHM of 0.0051 nm, corresponding to a Q-factor of 95,000. The regular shape of the recorded peaks for this example indicates that the radius of the microdroplet is being tuned precisely between each data point on the curve; we can therefore convert the wavelength tuning precision (of the order of $\sim$0.001 nm here) to a radius tuning precision of the order of $\lesssim$1 Å.

The Q-factor measurement in Figure 5(*b*) can, in principle, be affected by the fluctuations in the ambient atmosphere of the humidity chamber and by heating caused by the absorption of the blue laser. Their influence was probed by recording two additional consecutive photothermal spectra using integration times of 400 ms and 500 ms (Figures 5*c* and 5*d*). The associated Q-factors were found to differ less than 3% compared to the previous value. The total time elapsed and spectral drifts observed between Figures 5(*b*)–5(*c*) and 5(*c*)–5(*d*) are 290 s and 312 s, and 0.4 nm and 0.3 nm, respectively.

Assuming uniform spectral drifts throughout each experiment is not consistent with these observations, as this would have imposed a significant increase in the peak widths in Figures 5(*c*) and 5(*d*) compared to 5(*b*). We therefore conclude that the spectral drift has a low value while scanning the peak. We can assume that the observed overall drift is the result of low amplitude random fluctuations, or consists in a deterministic phenomenon that takes place at other times. We note that for different microdroplets we have observed spectral drifts in different directions between consecutive experiments, again with little difference in the measured Q-factors for each microdroplet at different integration times. This also excludes

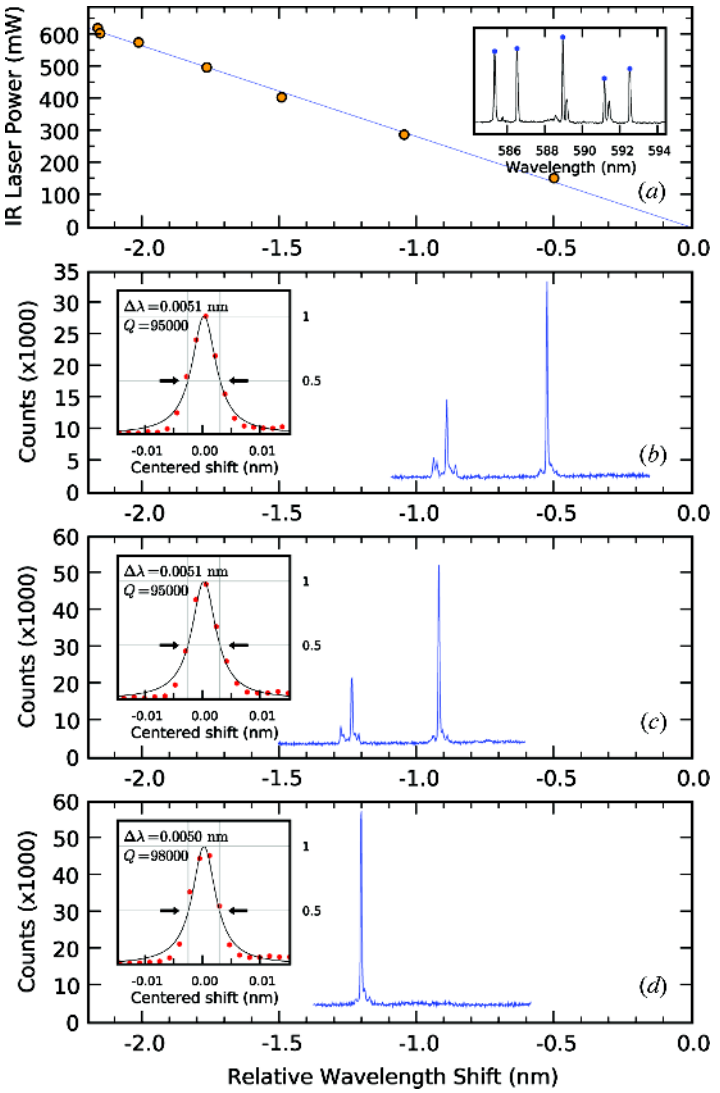

Figure 5. Succesive spectra taken from a 12 μm diameter microdroplet having a Q-factor of ~95,000. (*a*) Calibration data showing the linear dependence of the wavelength shift on the infrared laser power, converted to the probe wavelength $\lambda_p = 488$ nm. The spectra in (*b*)–(*d*) are taken with 250, 400, and 500 ms integration times, respectively. The observed spectral drift is attributed to the thermal instability of the chamber. Inset in (*a*) shows a sample spectrum from the calibration experiments. Detailed view of the high-Q peak and the FWHMs are shown in the insets of (*b*)–(*d*). (Figure is provided in color online.)

the possibility that the drift observed is caused by large random fluctuations. We speculate that these effects may be caused by random instabilities consecutive to the sudden blocking of the infrared laser after each measurement.

In the same way, the results presented in Figure 5 using different integration times exclude a significant contribution of heating caused by the absorption of the

blue laser to the measured Q-factors, since such a heating would have increased these values noticeably. In the regime where the absorption of the blue laser plays a role, we would expect the Q-factors to artificially increase at larger integration times due to the heating-induced evaporation of the microdroplet. This is, however, not observed in the results presented in Figure 5. For different microdroplets we have performed control experiments at different blue laser intensities, and observed an increase in the measured Q-factors with the blue laser intensity. The results shown in Figure 5 were performed using lower blue laser powers in the regime where blue laser absorption did not have a significant influence on these values.

During the experiments some peaks were oberved to exhibit an asymmetric profile, deformations at the base, or a clustering of peaks that cannot be explained

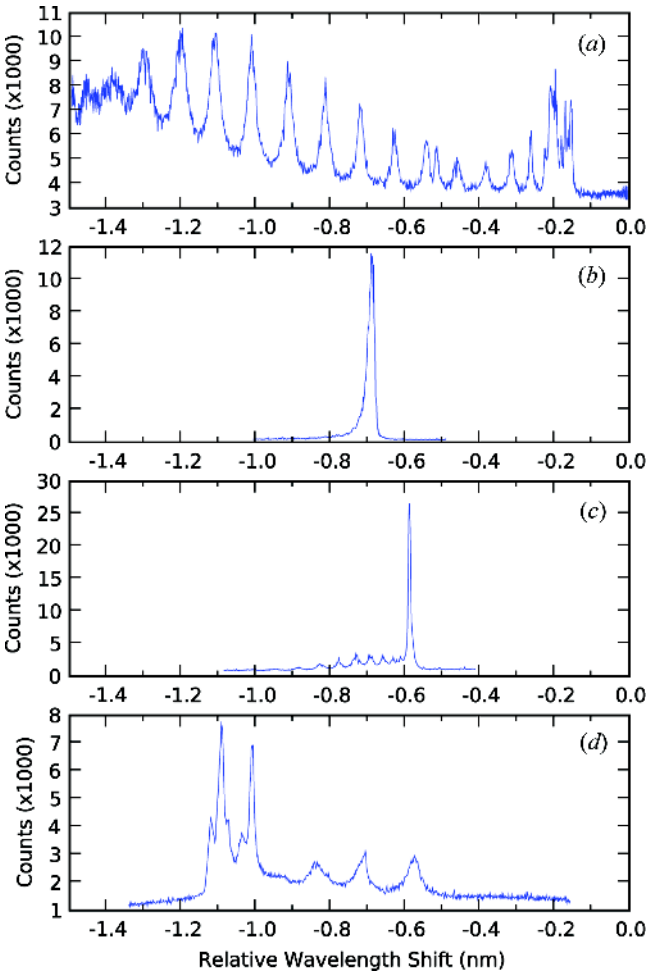

Figure 6. Spectra of non-ideal microdroplets. Observation of (*a*) the azimuthal degeneracy lifting of the WGMs, and (*b*) an azimuthally degenerate asymmetric low quality WGM. (*c*) and (*d*) show WGM peaks with more complicated structures. Integration times are 250 ms for (*a*)–(*d*). Microdroplet diameters are 13 μm in (*a*), (*c*), (*d*), and 9.5 μm in (*b*). (Figure is provided in color online.)

by the expected free spectral range of the observed WGMs. Figure 6 shows some examples of such non-ideal peaks. In Figure 6(*a*), a comb of peaks is observed that shows the distinctive features of WGMs whose azimuthal degeneracy has been lifted by a deformation of the microdroplet towards a spheroid (Yorulmaz et al. 2009). Figure 6(*b*) shows what seems to be a single wide and asymmetric peak that consists of several degeneracy-lifted azimuthal modes whose wavelength separation is beneath our resolution. Figures 6(*c*) and 6(*d*) show non-ideal peak shapes that cannot be interpreted simply. For all the microdroplets discussed in Figure 6, no obvious deviations from a truncated spherical geometry were observed in the images recorded from the microscope viewfinder. Despite this, the WGMs observed in the corresponding photothermal spectra revealed largely asymmetric profiles that we mainly attribute to nonisotropic changes in the light path due to deformations of the microdroplets (Yorulmaz et al. 2009), and to the optical coupling to the dielectric substrate (Le Thomas et al. 2006).

The photothermal tuning spectroscopy method thus allows us to measure the *Q*-factors of WGM resonances of salt-water microdroplets at wavelengths for which a tunable laser may not be available. The tuning range is also potentially greater than that of a tunable laser, as demonstrated earlier for the photothermal tuning effect (Kiraz et al. 2009). The well-resolved peaks observed indicate that the size of microdroplets can be tuned with a high precision (<1 Å) for several seconds, which also validates the use of the humidity chamber to establish stable experimental conditions.

5. PHOTOTHERMAL SELF-STABILITY USING ABSORPTION RESONANCES

Hysteretic behavior and photothermal self-stability are observed when the infrared heating laser is focused near the rim of a microdroplet. Figure 7 shows the spectral position of a WGM measured using the monochromator as a function of the incident infrared laser power (P_{inc}) during two consecutive photothermal tuning cycles, for a microdroplet exhibiting photothermal self-stability. In both cases, a horizontal plateau is observed where the spectral position of the WGM remains almost stable while P_{inc} is decreased from its maximum value. This position corresponds to a self-stable operation point. A small offset is observed between the consecutive hysteresis loops as P_{inc} is increased, due to slight fluctuations in the ambient atmosphere. Such an offset is not observed at the spectral position of the self-stable point, indicating that this point remains unaffected by the slight fluctuations. Additional proof of the self-stable operation is shown in Figure 8, where consecutive spectra recorded from a microdroplet using the monochromator are plotted in the absence (bottom) and presence (top) of self-stabilization. In both cases, the ambient atmosphere is perturbed by heating a wire resistor attached to the humidity chamber for 3 s at $\sim$10 W (see dashed lines in the figure). Following resistive heating, no change is observed in the spectral position of the WGMs in the presence of self-stabilization within our resolution. In contrast, considerable spectral drift is observed in the absence of self-stabilization (red shift by 5 nm).

The high precision of the self-stabilization mechanism is shown with fluorescence excitation experiments performed using the tunable laser. Figure 9 demonstrates the change in the rhodamine 700 fluorescence intensity recorded from a self-stabilized 15 μm diamater microdroplet using the APD during rough (bottom) and fine (top) scans of the tunable laser. During these measurements, the

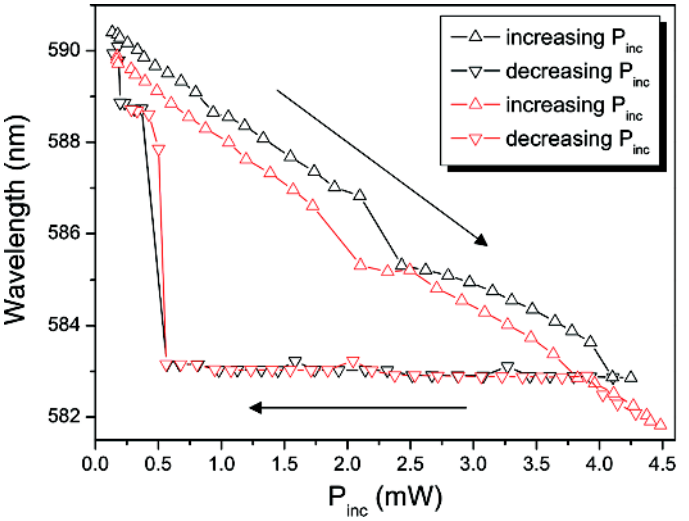

Figure 7. Two consecutive photothermal tuning cycles recorded from a 14 μm diamater microdroplet. The horizontal plateau observed in both hysteresis curves at 583.1 nm is due to the self-stable operation point. The difference between the initial and final positions in a hysteresis loop is due to the atmospheric fuctuations in the chamber. The sudden spectral jumps approximately 0.1 nm at around $P_{inc} = 0.78$ mW correspond to the multiline spectrum of the diode-pumped solid state infrared laser. (Figure is provided in color online.)

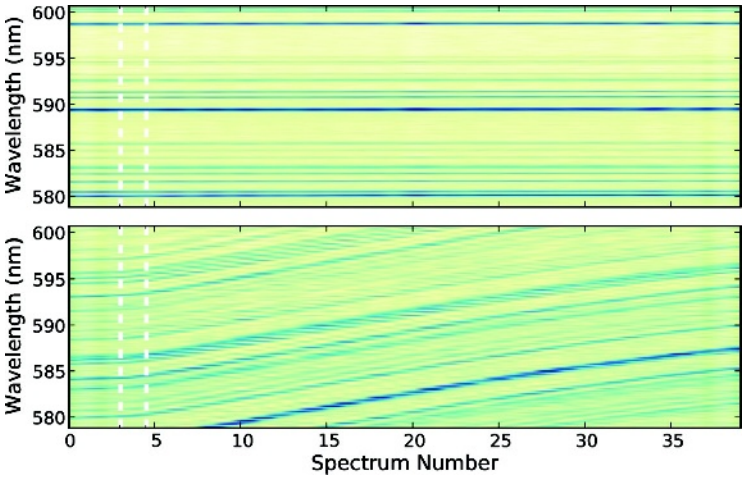

Figure 8. Contour plot of 40 consecutive spectra recorded from a 10 μm diameter NaCl-water microdroplet in the presence (top) and absence (bottom) of self-stabilization. The accumulation time between two consecutive spectra is 2.5 s. Dashed lines indicate the period of resistive heating. Due to resistive heating a red shift of 5 nm is observed in the WGMs in the absence of self-stabilization. (Figure is provided in color online.)

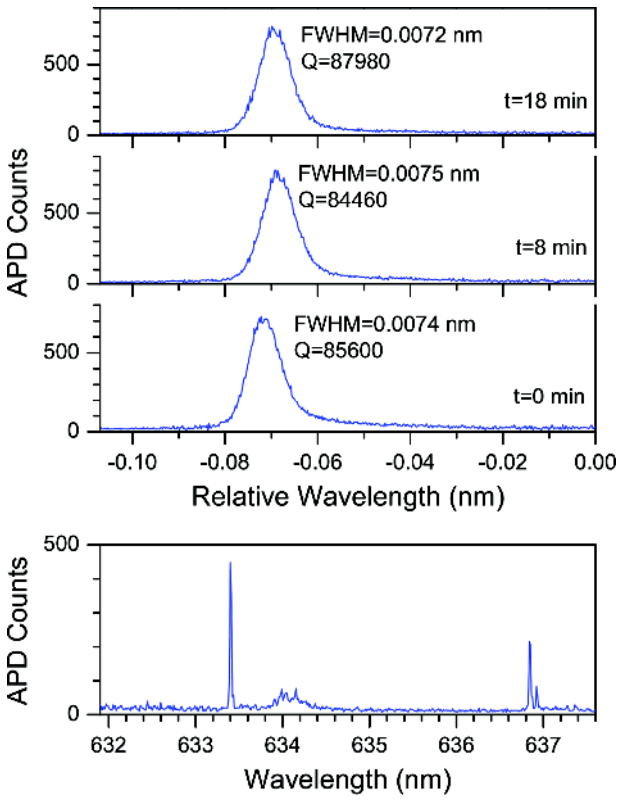

Figure 9. Fluorescence intensity recorded from a self-stabilized rhodamine 700 doped 15 μm diamater microdroplet during rough (bottom) and fine (top) scans of the tunable laser, using 30 ms integration time. Initial wavelength is selected to be 633.45 nm for the fine scans. Consecutive fine scans recorded at 0, 8, and 18 min show that the quality factor of this microdroplet is ~85,000 at all times and the lineshape is well preserved. Spectral drift within 18 min is less than 0.004 nm, showing the high precision of the self-stabilization mechanism. (Figure is provided in color online.)

microdroplet was kept at a self-stable operation point at all times. The rough scan shows the WGM observed at around 633.4 nm. This WGM is monitored with a higher resolution with consecutive fine scans performed starting from a wavelength of 633.45 nm. During an 18 min time interval, no considerable deviation is observed in the spectral position and lineshape of the WGM. The FWHM of the WGM resonance is preserved within 0.0072–0.0075 nm (corresponding to a Q-factor of ~85,000), while the spectral position is observed to drift by less than 0.004 nm. These imply stabilization of the radius of the microdroplet within <1 Å during 18 min.

6. CONCLUSIONS

We have demonstrated how the photothermal effect can be used to tune and lock the size and WGM spectrum of salt-water microdroplets standing on a superhydrophobic surface in a humidity chamber. Both tuning and locking rely

on the same fundamental mechanism that is the absorption of light by water molecules in the microdroplet, leading to a deviation from the equilibrium size by reversible local heating-induced evaporation. The position and orientation of the laser used for local heating relative to the microdroplet are crucial, as they determine how the absorption efficiency $\widetilde{Q}_{\text{abs}}$ changes as a function of the microdroplet size parameter α.

For on-axis illumination (heating laser focused to the center of the microdroplet), $\widetilde{Q}_{\text{abs}}$ is a slowly oscillating function of α with a low amplitude, enabling to tune the microdroplet size linearly by adjusting the heating laser power. We have shown how photothermal tuning could be used to record WGM spectra of microdroplets and measure Q-factors of up to $\sim 10^5$ at 488 nm for azimuthally degenerate WGM resonances, without necessitating a tunable laser. Our measurements using photothermal tuning spectroscopy revealed a one order of magnitude improvement over the conventional fluorescence spectroscopy experiments with microdroplets using a monochromator. These results also indicate that the achieved size tuning precision is of the order of ~ 1 Å over several seconds. The achieved tuning resolution does not constitute a fundamental limitation, it could be increased by using a more precise rotation stage with more steps per revolution.

For off-axis illumination, with the heating laser focused at the rim of the microdroplet, $\widetilde{Q}_{\text{abs}}$ exhibits sharp WGM resonances as a function of α. These resonances lead to a hysteretic behavior as the heating laser power is increased and decreased in a cycle. Such a behavior enables microdroplets to be used as optically bistable elements whose resonances can be switched between two wavelengths in a reproducible way. Furthermore, the low-wavelength part of the hysteresis curve corresponds to a self-stable operation regime for the microdroplets, rendering their size and WGM spectrum resilient to external perturbations. We have demonstrated various aspects of such a locking effect, in particular how it can be used to stabilize the WGM spectrum within ~ 0.01 nm (corresponding to a size stabilization of ~ 1 Å) for several minutes. This enabled us to characterize WGM resonances with the fine scan feature of a tunable laser in a reproducible fashion, confirming the order of magnitude of the Q-factors measured by photothermal tuning spectroscopy.

In conclusion, we have shown how to overcome some of the challenges inherent to using liquid microdroplets as optical resonators, namely tuning and stabilizing their WGM spectrum. Their cost-effective and easy to produce nature could make them attractive alternatives to solid microcavities for applications such as tunable lasers and quantum optics experiments. This work may also be a first step towards their use in cavity optomechanical experimental, such as cooling mechanical motion through the coupling of optical and mechanical modes (Kippenberg and Vahala 2007). The liquid nature of microdroplets may enable higher optomechanical coupling coefficients than for solid optical microcavities, which could prove to be important in such studies. Furthermore, they may offer new possibilities for high performance intra-cavity chemical and biological sensing experiments.

ACKNOWLEDGMENTS

The authors thank the Alexander von Humboldt Foundation for equipment donation. A. Kiraz acknowledges the financial support of TÜBA in the framework

of the Young Scientist Award program (TÜBA-GEBIP). M. Mestre acknowledges partial support from TÜBİTAK and the Koç University postdoctoral fellowship program.

REFERENCES

The Engineering Toolbox. http://www.engineeringtoolbox.com/ (accessed September 15, 2009).

Fields, M. H., J. Popp, and R. K. Chang. 2000. *Nonlinear Optics in Microspheres*. Vol. 41. Amsterdam: Elsevier.

Gouesbet, G. and J. A. Lock. 1994. Rigorous justification of the localized approximation to the beam-shape coefficients in generalized Lorenz–Mie theory. II. Off-axis beams. *J. Opt. Soc. Am. A* 11(9):2516–2525.

Karadag, Y., M. Mestre, and A. Kiraz. 2009. Photothermal self-stability and optical bistability of a NaCl-water microdroplet on a superhydrophobic surface. *Phys. Chem. Chem. Phys.* 11(33):7145–7151.

Kippenberg, T. J. and K. J. Vahala. 2007. *Opt. Express* 15(25):17172–17205.

Kiraz, A., A. Kurt, M. A. Dündar, and A. L. Demirel. 2006. Simple largely tunable optical microcavity. *Appl. Phys. Lett.* 231(8):081118.

Kiraz, A., Y. Karadağ, and M. Muradoğlu. 2008. Large spectral tuning of a water/glycerol microdroplet by a focused laser: Characterization and modeling. *Phys. Chem. Chem. Phys.* 10(42):6446–6454.

Kiraz, A., Y. Karadag, S. C. Yorulmaz, and M. Muradoglu. 2009. Reversible photothermal tuning of a salty water microdroplet. *Phys. Chem. Chem. Phys.* 11(15):2597–2560.

Lock, J. A. and G. Gouesbet. 1994. Rigorous justification of the localized approximation to the beam-shape coefficients in generalized Lorenz–Mie theory. I. On-axis beams. *J. Opt. Soc. Am. A* 11(9):2503–2515.

McHale, G., S. Aqil, N. J. Shirtcliffe, M. I. Newton, and H. Y. Erbil. 2005. Analysis of droplet evaporation on a superhydrophobic surface. *Langmuir* 21(24):11053–11060.

Orrit, M. and J. Bernard. 1990. Single pentacene molecules detected by fluorescence excitation in a p-terphenyl crystal. *Phys. Rev. Lett.* 65(21):2716–2719.

Picknett, R. G. and R. J. Bexon. 1977. The evaporation of sessile or pendant drops in still air. *J. Colloid Interface Sci.* 61(2):336–350.

Qian, S.-X., J. B. Snow, H. M. Tzeng, and R. K. Chang. 1986. Lasing droplets: Highlighting the liquid–air interface by laser emission. *Science* 231(4737):486–488.

Ray, A. K., R. D. Johnson, and A. Souyri. 1989. *Langmuir* 5(1):133–140.

Reid, J. P., H. Meresman, L. Mitchem, and R. Symes. 2007. Spectroscopic studies of the size and composition of single aerosol droplets. *Int. Rev. Phys. Chem.* 26(1):139–192.

Tang, I. N., A. C. Tridico, and K. H. Fung. 1997. Thermodynamic and optical properties of sea salt aerosols. *J. Geophys. Res.* 102(D19):23,269–23,275.

Le Thomas, N., U. Woggon, W. Langbein, and M. V. Artemyev. 2006. Effect of a dielectric substrate on whispering-gallery-mode sensors. *J. Opt. Soc. Am. B* 23(11):2361–2365.

Tzeng, H.-M., K. F. Wall, M. B. Long, and R. K. Chang. 1984. Evaporation and condensation rates of liquid droplets deduced from structure resonances in the fluorescence spectra. *Opt. Lett.* 9(7):273–275.

Vahala, K. J. 2003. Optical microcavities. *Nature* 424(6950):839–846.

Yorulmaz, S. C., M. Mestre, M. Muradoglu, B. E. Alaca, and A. Kiraz. 2009. *Opt. Comm.* 282(14):3024–3027.